

Dynamic evolution of low-viscosity fuel particle distribution driven by constant flow

Zhong-Kun Yang(杨仲坤), Gao-Jun An(安高军), Xi-Meng Xu(徐曦萌), Zhe Zheng(郑哲), Yong-Xu Wang(王永旭), Li-Feng Xie(解立峰), Dan Zhang(张丹), and Bin Li(李斌)

Citation: Chin. Phys. B, 2023, 32 (**7**): 074701. DOI: 10.1088/1674-1056/acc8c2

Journal homepage: http://cpb.iphy.ac.cn; http://iopscience.iop.org/cpb

What follows is a list of articles you may be interested in

Nanobubbles produced by hydraulic air compression technique

Xiaodong Yang(杨晓东), Qingfeng Yang(杨庆峰), Limin Zhou(周利民),Lijuan Zhang(张立娟), and Jun Hu(胡钧)

Chin. Phys. B, 2022, 31 (**5**): 054702. DOI: 10.1088/1674-1056/ac464c

Crown evolution kinematics of a camellia oil droplet impacting on a liquid layer

Zhongyu Shi(石中玉), Guanqing Wang(王关晴), Xiangxiang Chen(陈翔翔), Lu Wang(王路), Ning Ding(丁宁), and Jiangrong Xu(徐江荣)

Chin. Phys. B, 2022, 31 (**5**): 054701. DOI: 10.1088/1674-1056/ac46c1

Effect of viscosity on stability and accuracy of the two-component lattice Boltzmann method with a multiple-relaxation-time collision operator investigated by the acoustic attenuation model

Le Bai(柏乐), Ming-Lei Shan(单鸣雷), Yu Yang(杨雨), Na-Na Su(苏娜娜), Jia-Wen Qian(钱佳文), and Qing-Bang Han(韩庆邦)

Chin. Phys. B, 2022, 31 (**3**): 034701. DOI: 10.1088/1674-1056/ac2b93

Numerical simulation on partial coalescence of a droplet with different impact velocities

Can Peng(彭灿), Xianghua Xu(徐向华), and Xingang Liang(梁新刚)

Chin. Phys. B, 2021, 30 (**5**): 054703. DOI: 10.1088/1674-1056/abd7dd

Investigation of cavitation bubble collapse in hydrophobic concave using the pseudopotential multi-relaxation-time lattice Boltzmann method

Minglei Shan(单鸣雷), Yu Yang(杨雨), Xuemeng Zhao(赵雪梦), Qingbang Han(韩庆邦), and Cheng Yao(姚澄)

Chin. Phys. B, 2021, 30 (**4**): 044701. DOI: 10.1088/1674-1056/abcf4b

---

Dynamic evolution of low-viscosity fuel particle distribution driven by constant flow

Zhong-Kun Yang(杨仲坤)[1], Gao-Jun An(安高军)[2], Xi-Meng Xu(徐曦萌)[2], Zhe Zheng(郑哲)[2], Yong-Xu Wang(王永旭)[1], Li-Feng Xie(解立峰)[1], Dan Zhang(张丹)[1], and Bin Li(李斌)[1,†]

[1] *School of Chemistry and Chemical Engineering, Nanjing University of Science and Technology, Nanjing* 210000, *China*
[2] *Institute of Systems Engineering, AMS, PLA, Beijing* 100000, *China*

(Received 18 January 2023; revised manuscript received 20 March 2023; accepted manuscript online 30 March 2023)

The effects of mass concentration and injection pressure on the atomization characteristics of low-viscosity fuel spray are studied in a constant-volume chamber. Microscopic spray parameters are measured by laser diffraction at different axial and radial positions downstream of the nozzle. The results show that the atomization effect is inhibited linearly with the increase of mass concentration. The increase of injection pressure promotes the droplet breakup. However, the trend gradually weakens and becomes more noticeable at high concentrations. Comparing with the concentration, the influence of the injection pressure on the atomization characteristics is dominant. Although low concentration and high injection pressure can promote the droplet breakup, they also increase the probability of droplet collision, resulting in droplet aggregation. This is more evident in low-viscosity fuels. The droplet size increases in the axial direction owing to the aggregation. However, the diameter decreases in the radial direction owing to the outward deflection of small droplets caused by air turbulence and entrainment. In addition, the high-velocity airflow significantly promotes the droplet breakup near the nozzle and spray axis regions and inhibits the aggregation effect. However, the lower-viscosity fuels keep smaller droplet sizes and better atomization in the whole spraying process, which is easier to realize than the higher-viscosity fuels. Overall, low concentration, high injection pressure, and low viscosity of fuel have beneficial effects on the droplet breakup. This is very important for improving the atomization effect of fuel.

Keywords: low-viscosity fuel, spray and atomization, particle distribution, laser diffraction

PACS: 47.55.Ca, 62.50.–p, 52.57.Fg **DOI:** 10.1088/1674-1056/acc8c2

1. Introduction

With the rapid development of global modernization and industrialization, the dependence on fuel and demand for it have increased. Low-viscosity fuels have been widely used as alternative energy sources and fuel additives for internal combustion engines owing to their inherent advantages.[1–3] Compared with high-viscosity fuels, they can provide good fuel economy.[4] Moreover, they exhibit significant advantages in improving emission quality, reducing fuel consumption, increasing machine power, and reducing failure and maintenance rates.[5,6] The fuel spray and atomization characteristics are the main factors affecting the combustion and emission performances of internal combustion engines.[7] Good dispersion atomization can affect the fuel distribution in the burner to a certain extent, thereby improving the ignition,[8] combustion,[9] and emission characteristics[10,11] of the fuel. Moreover, the formation of fuel–air mixture, which is an important factor in controlling the combustion rate to reduce emissions, is influenced by the fuel atomization characteristics. Reitz and Duraisamy[12] and Biswas *et al.*[13] found that a shorter mixing time of fuel and air can improve engine performance to some extent. Effective fuel combustion depends on an effective atomization process.[14] This is determined by the physicochemical qualities of the fuel and the injection settings.[15]

Several studies have been conducted to determine the spray properties of gasoline and diesel fuels;[16,17] however, some disagreement about the macroscopic behavior still exists. In the process of fuel injection and atomization, owing to the strong aerodynamic force, the fuel is broken and atomized almost instantaneously; therefore, it is necessary to have a clear and accurate understanding of the microscopic characteristics of the physical process of the spray and to conduct a comprehensive study of its atomization process and cloud development.[18] The droplet size after spraying is a key parameter for evaluating the atomization performance from a microscopic perspective.[19,20] Park *et al.*[21] studied the atomization characteristics of gasoline and diesel fuel blends and showed that the fuel droplet size decreases, the ignition delay time increases, and the NO_x and soot emissions decreases.

Han *et al.*[22] also conducted an experimental study of the spray characteristics of diesel and gasoline fuel blends, but they mainly focused on the effects of the proportion of gasoline on volume and mass injection rates and spray cone angle. In their study Kim *et al.*[23] obtained the conclusion that narrower spray cone angle has better performance in terms of maximum combustion pressure, maximum heat release rate and ignition delay. It is advantageous under the early com-

†Corresponding author. E-mail: libin@njust.edu.com

© 2023 Chinese Physical Society and IOP Publishing Ltd

bustion strategy. However, the spray penetration decreases and the spray width increases, which promotes the mixing of fuel and gas. This was mainly attributed to the blending of low viscosity fuel additives.[24] Lin *et al.*[25] combined the microscopic measurement means of a phase Doppler particle analyzer to study the characteristics of a liquid spray under the action of high-speed airflow. They found that the local droplet size of the distribution of clouds significantly affects the overall cloud spray characteristics. By determining the time-averaged properties of the spray, the researchers converted the droplet diameters in the center of the axial flow into the surface at the measurement points on the cross-section. Kannaiyan and Sadr[26] used a laser diagnostic measurement technique for spray experiments on jet fuel under ambient atmospheric conditions and reported the effect of particle size parameters on the microscopic spray performance. Recently, they compared the microscopic spray characteristics of jet fuel in spray chambers.[27] The droplet states in different regions of the spray process were derived from the measurements at the different spray axial positions. Chang *et al.*[28] investigated droplet behavior under ultra-high injection pressure conditions by using a particle image analysis detection technique. Parameters, such as the Sauter mean diameter (SMD/D_{32}) and droplet number, were used to evaluate the spray atomization characteristics.[29] Most of studies have been performed in constant-volume containers. Some researchers have also studied the volume of the test container, arguing that the constant volume of the closed chamber affects the atomization characteristics of the liquid.[30] Some researchers also used the principle of maximum entropy and the law of conservation of mass to deduce and study the droplet size and distribution, and they used models to predict the droplet formation characteristics of diesel sprays.[31–34] From all the findings they concluded that the spray performance is closely related to the microscopic behavior of the droplets in the spraying process and cloud development,[35] which would serve as the key motivation for this study.

In contrast, fuels can form mixtures with air in the event of a leakage during production, storage, and transportation. The mixture has a risk of explosion when exposed to an ignition source. Especially in high-pressure situations, such as broken pipes and containers, fuel injection, accompanied with high-speed air flow, may make spray explosions more likely to occur.[36–38] However, there is little research on low-viscosity fuels. Liu *et al.*[39] emphasized the necessity of investigating the spray particle size. They investigated the effect of the diameter of *n*-hexane on the explosion characteristics of its mixture with air. Both the explosion pressure and temperature, which represent the explosion hazard, were inversely associated with the particle size of the cloud. Lyu *et al.*[40] found that the variation in the SMD has a remarkable effect on the explosion characteristics. Particle size also affects the ignition sensitivity. Recently, Wu *et al.*[41] investigated the atomization and spray explosion properties of methanol based on a 20L spherical container. The variations in the spray particle size measured by the laser diffraction technique are consistent with the changes of explosion pressure.

Therefore, from the perspective of improving combustion performance or preventing explosion accidents, it is worthy of attention to evaluate the microscopic atomization performance by the droplet size after spraying.[42] At present, studies mainly focus on measurements under fixed-test conditions, with research and exploration of the combined effects of multiple factors lacking. Existing studies have paid insufficient attention to the spray characteristics of low-viscosity fuels, so it is necessary to investigate their atomization characteristics and cloud development status in depth and detail. To this end, in this work we study and compare the combined effects of the fuel mass concentration (ratio of fuel mass to spray chamber volume, c = 200, 400, 600, 800, and 1000 g/m^3) and injection pressure (pressure of the driving airflow at the fuel inlet, p_{i} = 0.50, 0.75, 1.00, 1.25, 1.50, and 2.00 MPa) on low-viscosity fuels under ambient conditions of 1 atm (1 atm = 1.01325×10^5 Pa) and 20 °C. The fuel droplet size parameters are measured by using laser diffraction techniques, and the droplet formation characteristics of different types of low-viscosity fuels are compared at several axial and radial measurement positions downstream of the nozzle outlet.

This study fill the gaps in the atomization characteristics and spray development mode of low-viscosity fuel, and provides references for improving combustion performance and avoiding accidental disasters.

2. Experimental setup and methods

2.1. Experimental setup

The spray tests were conducted in a 20-L spherical container as shown in Fig. 1. The inner diameter of the spray chamber was 340 mm, and the thickness of the wall was 10 mm. The device was equipped with two quartz optical windows (each with an observation diameter of 100 mm), a pneumatic atomization system, cooling circulation system, and terminal control system. The centers of the two optical windows were aligned on the same level as the center of the spray chamber, which was used for better optical and laser diagnostic measurements. Owing to the presence of optical windows and material limitations, the maximum pressure bearing limit of the spray chamber was 2 MPa. The nozzle was installed at the same level as the center of the spray chamber, while the two optical windows were orthogonal to the vertical axis of the nozzle (see Fig. 1). The nozzle was connected to the sample chamber by an explosion-proof solenoid valve. The sample

chamber was pressurized with high-pressure air and injected through the nozzle at the required pressure. The pneumatic atomization system was equipped with a pressure sensor to monitor the injection pressure.

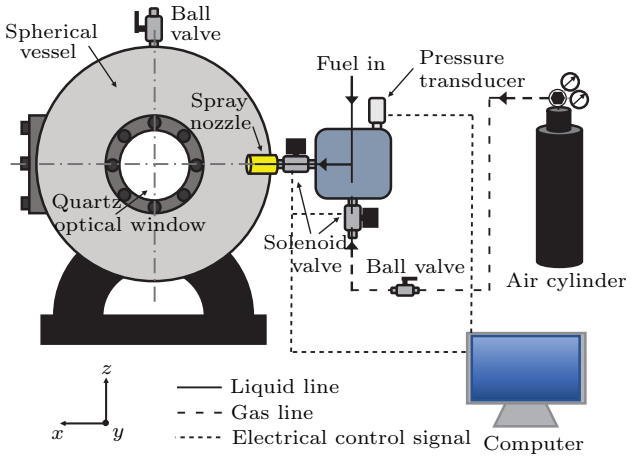


Fig. 1. Schematic diagram of the experimental setup.

2.2. Optical/laser diagnostic measurement

A laser diffraction (LD) system from Malvern Panalytical Spraytec was used for point-by-point measurements of the spray particle and droplet size distributions in real time. The LD system used for the experimental measurements is illustrated in Fig. 2. It was equipped with a highly stable He–Ne laser, a transmitter, a receiver, an optical bench, and a signal processing software. The system used the laser diffraction principle to measure the particle size by measuring the intensity of the diffracted light as the laser beam passed through the spray. Subsequently, the size of the droplets that created the diffraction pattern was analyzed and calculated based on Mie theory[43–45] and Fraunhofer scattering optical model. For the LD system with a red parallel laser of wavelength $\lambda = 633$ nm, a quartz glass with light transmission wavelength in the range 633 ± 10 nm and transmission $\geq 98\%$ was used to eliminate interference from other wavelengths to achieve the optimal measurement accuracy.[37,39] The operating parameters of the LD system are presented in Table 1.

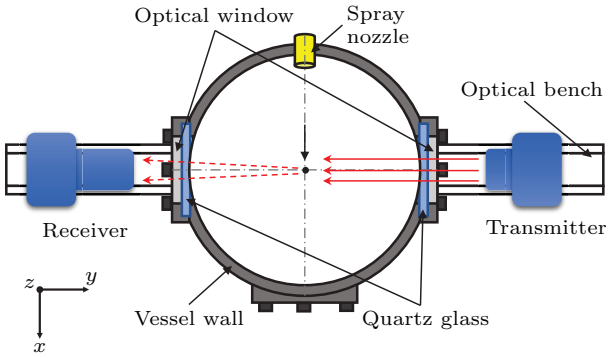


Fig. 2. The LD system.

Table 1. Operating parameters of the LD system.

General		Optics		Sizing performance	
Acquisition mode	rapid mode	light source	Max 4 mW He–Ne laser	particle size	2 μm–2000 μm
Data acquisition rate	2.5 kHz	lens arrangement	Fourier (parallel beam)	accuracy	better than 1%
Maximum measurement time	30 s	lens focal length	750 mm	repeatability	better than 1%

2.3. Materials

Considering the viscosity characteristics of the fuel, a low-viscosity fuel with viscosity less than 3 mPa·s was used for the experiments in this study. 1-butanol and cyclooctane were used as fuel substitutes and additives, which can increase the calorific value of fuel and improve the combustion efficiency, providing better fuel economy than traditional fuel economy. Also, they can effectively reduce the carbon smoke emission in the combustion process under the same quality, which is strategically important in energy saving and emission reduction. The properties of the experimental materials are presented in Table 2.

Table 2. Properties of experimental materials.

Properties at 293 K, 1 atm	1-butanol	Cyclooctane	Water
Density (kg/m^3)	0.810	0.835	0.998
Boiling point (°C)	117	149	100
Viscosity (mPa·s)	2.95	2.17	1.01
Surface tension (mN/m)	25.4	25.9	72.8
Refractive index	1.399	1.458	1.333

2.4. Methods

The experiments were conducted under the following environmental conditions: the initial ambient pressure in the spray chamber was 0.10 MPa, and the initial ambient temperature and fuel temperature were maintained at 293 K by using the cooling circulation system. The particle size measurement experiments were performed according to the following steps. (i) The spray chamber and quartz optical glasses were cleaned. (ii) Fuel was added into the sample chamber. (iii) The control system was initialized. The air inlet solenoid valve was opened, and high-pressure air was injected into the sample chamber. The air inlet solenoid valve was closed when the pressure reached the preset spray pressure. (iv) The spray solenoid valve was opened (continuous opening time was set to 100 ms), and the fuel was sprayed from the nozzle together with the high-speed airflow. (v) The Spraytec LD system was automatically triggered off, which tested and collected data. (vi) The chamber was cleaned and flushed repeatedly with dry air. Each spray measurement was performed after the envi-

ronmental and operating conditions had reached a stable and uniform state.

The particle size measurements in this study were performed downstream of the nozzle outlet at different axial (x) and vertical radial (z) positions, as shown in Fig. 3. Because the laser measurement range was limited, the optical bench was adjusted to obtain measurements at different positions. The radial orientation on one side was selected for the measurement because the spray was axially symmetric about the spray direction.

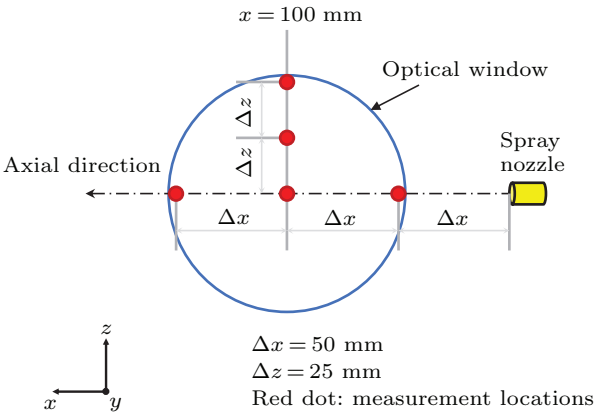


Fig. 3. Details of particle size measurement locations.

2.5. Experimental uncertainty analysis

The experimental uncertainty in the results of the spray characteristics primarily arises from the test apparatus, fuel addition, initial ambient pressure, and initial ambient temperature. The LD system is based on Mie theory, where large and small particles are diffracted against the laser at small and large angles, respectively. Thus, the particle size was determined by the intensities of the diffracted light at different angles. The measurement of the ambient background before the experiment contributed to the accuracy of the experimental data. However, the uncertainty of the particle size measurement was confirmed to be under 5% by using a monodisperse droplet generator. Samples were added by using a pipette with an accuracy of 1% and volume rang of 0 mL–50 mL in this study. Thus, the fuel content in the sample chamber was estimated to have a maximum uncertainty of ± 0.5 mL. The initial ambient pressure was measured by using a pressure gauge with an accuracy of 1.6% in the pressure range of 0 MPa–1 MPa. The initial ambient temperature was measured by using a digital electronic thermometer with an accuracy of 1% in the temperature range of 263 K–363 K. Therefore, the pressure and temperature measurements in this study displayed maximum errors of ± 16 kPa and ± 1 K, respectively.

3. Results and discussion

The droplet size distribution of a spray is a critical indicator in the evaluation of atomization characteristics. To characterize the fineness and uniformity of the fuel spray, the arithmetic mean droplet diameter (D_{10}) and Sauter mean diameter (SMD/D_{32}), which are of significance for the combustion industry, are quantified and compared.[46]

3.1. Variations of spray particle size under effects of mass concentration and injection pressure

Experiments on 1-butanol spray parameters, including droplet diameter and size distribution, are conducted with variations in fuel mass concentration and injection pressure. Figure 4 presents a comparison among the particle sizes of the 1-butanol spray as a function of mass concentration at various injection pressures. As shown in Fig. 4(a), the diameter of the 1-butanol droplet increases with the concentration increasing, and the variation in D_{10} presents a good linear fit. The statistical information of the linear fit curves is shown in Table 3. This trend is consistent for all the cases investigated under this condition. At $p_i = 0.50$ MPa, the diameter of 1-butanol at a concentration of 1000 g/m^3 is the largest, 1.85 times larger than that at 200 g/m^3. The increase in the concentration weakens the driving force of the spray airflow per unit mass of fuel, causing the spray velocity at the nozzle exit to decrease. Further analysis shows that the decrease in the turbulence intensity leads the droplet diameter to increase. This implies that fuel with lower concentration has better atomization. As the injection pressure increases, the droplet size decreases for the same concentration 1-butanol. The maximum difference in D_{10} between $p_i = 0.50$ MPa and 2.00 MPa is observed at the concentration of 1000 g/m^3, which is reduced by 77.55%. This phenomenon can be explained based on dimensionless analysis, where the augment of the injection pressure increases the Mach number (Ma) of the airflow under the condition of constant ambient pressure, resulting in a larger driving force. The resulting increase in the Weber number (We) promotes the generation of small droplets of the spray. Furthermore, figure 4(a) shows that with the increase of the injection pressure, the effect of the change in concentration has less significant effect on D_{10}. As the injection pressure rises from 0.50 MPa to 2.00 MPa, the slope of the fitted curve of D_{10} *versus* concentration drops from 0.00864 to 0.00163, which is a reduction of 81.1%. The differences in D_{10} among the sprays at different concentrations decrease as the injection pressure increases. Therefore, a higher fuel concentration requires a larger driving force to obtain smaller droplets, so as to promote the atomization effect. Likewise, a lower injection pressure is not sufficient to promote the fragmentation of the fuel droplets. It can be observed that under a low-pressure difference, the effect of fuel concentration on the droplet diameter is more significant.

Figure 4(b) shows the comparison of D_{32} of the 1-butanol spray with the rise of concentration under various injection

pressures, where D_{32} represents the more general average diameter of the fuel spray. Aside from at $p_i = 2.00$ MPa, the same variation trends for particle size as that for D_{10} are observed. It is noteworthy that the minimum value of the D_{32} curve for $p_i = 2.00$ MPa is observed at the maximum concentration, which is contrary to the trend of the other curves. In particular, at a low concentration, D_{32} at $p_i = 2.00$ MPa is higher than at other injection pressures. The reason for this is the fuel breaking into small droplets in the atomization process, which is also known as secondary atomization. However, the motion direction of the droplets in the spraying process is not definite, and the probability of collisions between the droplets is high. Thus, some small droplets reaggregate into big droplets during the dispersion, which is called the aggregation effect. Particularly, the combined effect of low concentration and high *Ma* airflow creates an extremely strong turbulence intensity, which causes a more unstable spray process, resulting in an increased probability of collision between droplets and an obvious aggregation effect. This theory is further confirmed by comparing the droplet size distribution with cumulative number percentage of 1-butanol at $p_i = 2.00$ MPa. This is consistent with the conclusion concluded by Zhang *et al.*[47] that the augment of injection pressure further increases the irregularity of the spray.

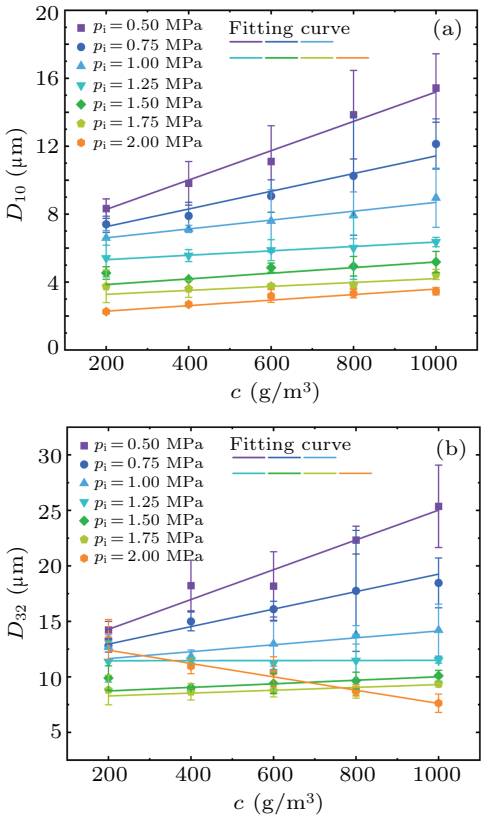


Fig. 4. Effects of mass concentration (c) on arithmetic mean droplet diameter (D_{10}, left) and Sauter mean diameter (D_{32}, right) of 1-butanol at different injection pressures (p_i) ($x = 100$ mm; $z = 0$ mm).

Figure 5 shows the droplet size distribution and cumulative number percentage for the cases $c = 200$ g/m^3 and 1000 g/m^3. At low concentration, the droplet size exhibits a shift toward smaller diameters, which demonstrates the decreasing trend of D_{10}. However, the collisional aggregation of droplets also results in the appearance of a small fraction of larger diameter droplets, which affects the D_{32} value to some extent. Thus, the low concentration of D_{32} appears to rise rather than drop at $p_i = 2.00$ MPa. The display in Fig. 5 further supports the above analysis.

Table 3. Statistical information for linear fit curves.

	p_i (MPa)	Fitting equation	R-squared
D_{10}	0.50	$y = 6.55 + 0.00864x$	0.99
	0.75	$y = 6.22 + 0.00521x$	0.94
	1.00	$y = 6.08 + 0.00261x$	0.98
	1.25	$y = 5.06 + 0.00129x$	0.99
	1.50	$y = 3.52 + 0.00166x$	0.73
	1.75	$y = 3.05 + 0.00116x$	0.81
	2.00	$y = 1.96 + 0.00163x$	0.98
D_{32}	0.50	$y = 11.60 + 0.01343x$	0.99
	0.75	$y = 11.38 + 0.00788x$	0.97
	1.00	$y = 11.02 + 0.00312x$	0.81
	1.25	$y = 11.44 + 0.00004x$	0.88
	1.50	$y = 8.41 + 0.00160x$	0.88
	1.75	$y = 8.03 + 0.00128x$	0.85
	2.00	$y = 13.61 - 0.00601x$	0.97

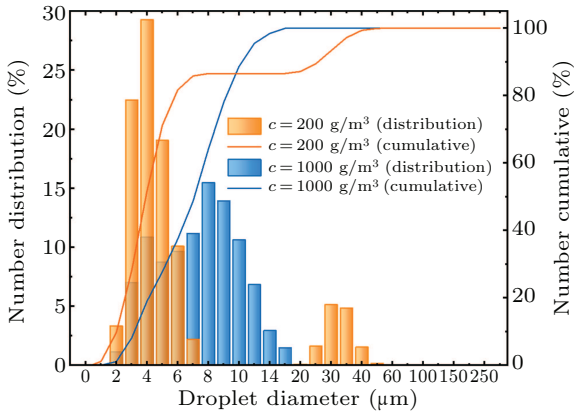


Fig. 5. Comparison of droplet size distribution and cumulative number percentage of 1-butanol spray for $c = 200$ g/m^3 and 1000 g/m^3 at $p_i = 2.00$ MPa ($x = 100$ mm; $z = 0$ mm).

The variation curves of the particle size with injection pressure for different concentrations of butanol and water spray are shown in Fig. 6. The arithmetic mean droplet diameter (D_{10}) is described as a function of the mass concentration and injection pressure as shown in Fig. 6(a). Both 1-butanol and water exhibit the best atomization effect for $p_i = 2.00$ MPa, and D_{10} drops to below 4 μm. Thus, aerodynamic forces remain dominant in the entire process of dispersion and atomization. Droplet fragmentation and atomization are improved with the increase of *Ma* of the airflow. Moreover, the values of D_{10} of 1-butanol decrease by 77.55% and 46.04% with the injection pressure and concentration increasing, respectively, and by 85.35% with the coupling effect increasing, while for water, the values of D_{10} of 1-butanol decrease

by 60.86%, 28.99%, and 59.27%, correspondingly. The low concentration and high injection pressure promote the fragmentation and atomization of the spray. However, the droplet particle sizes are relatively similar for different concentrations at the same injection pressure, thereby further demonstrating that the injection pressure is the main factor affecting the fuel spray, reducing the particle size to its limit, and weakening the concentration effect. However, the decreasing trend of D_{10} gradually decrease with injection pressure increasing, indicating that the injection pressure significantly contributes to the spray effect at high concentrations. Water exhibits a smaller D_{10} as shown in Fig. 6(a). This is because water has a lower viscosity than 1-butanol, and it is easier to break into small droplets after experiencing the same high-speed airflow, achieving a significant atomization effect. Furthermore, as *Ma* of the jet airflow increases, a smooth change in the particle size is observed earlier for water than for 1-butanol. This phenomenon is more obvious at low concentrations.

Figure 6(b) shows the comparison among the values of SMD (D_{32}) which is a function of the mass concentration and injection pressure for 1-butanol and water sprays. Majority of the data in the graph maintain the same trend as that for D_{10}. The droplet size distribution and cumulative number percentage explain this phenomenon more clearly as shown in Fig. 7(a). It can be observed that the droplet distribution of the fuel spray at $p_i = 2.00$ MPa shifts toward smaller sizes. The D_{10} and D_{32} decrease at higher injection pressures, which is mainly attributed to the contribution of the small droplets. This further confirms that a high injection pressure significantly promotes the droplet breakup. However, for 1-butanol droplets at low concentrations and high injection pressure, D_{32} appears to become larger, and the maximum value is observed at the minimum concentration. This is because the influence of low concentration and high *Ma* lead the *We* of the high-speed airflow to increase. Thus, the increase in the turbulence intensity results in the small droplets having a higher probability of aggregating into larger droplets. Figure 7(b) displays a visual illustration of the theory. The droplet size distribution and cumulative number percentage at low concentrations are presented. The high injection pressure promotes droplet breakup, resulting in the increase of the number of small droplets, which contributes to D_{10} decreasing. Droplet aggregation is also observed, and the increase of D_{32} is mainly caused by the contribution of the little fraction of large droplets. Similarly, D_{32} of the water spray demonstrates an increasing trend with injection pressure increasing. It should be noted that D_{32} values of water for $c = 600$ g/m^3 and 200 g/m^3 show increasing trends at $p_i = 1.5$ MPa and 1.25 MPa, respectively, compared with the variation observed for 1-butanol at $p_i = 2.00$ MPa.

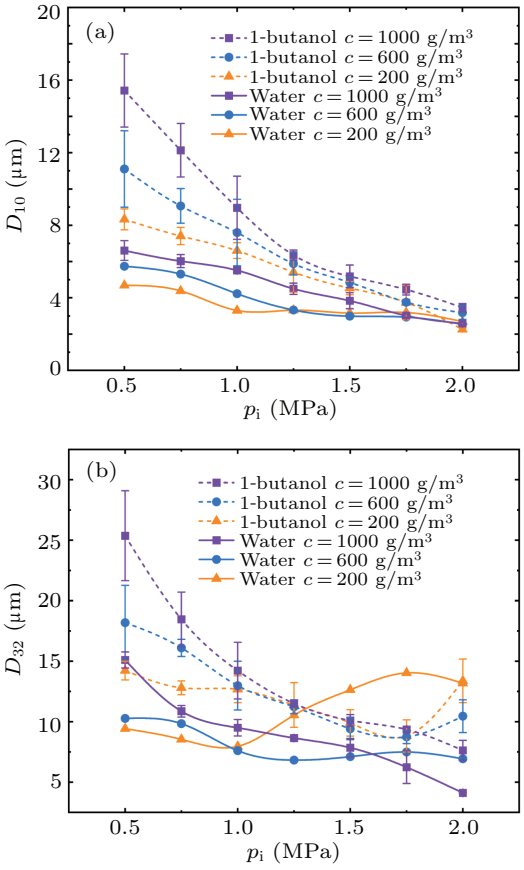


Fig. 6. Effects of injection pressure (p_i) on (a) arithmetic mean droplet diameter (D_{10}) and (b) Sauter mean diameter (D_{32}) of 1-butanol and water at different mass concentrations (c) ($x = 100$ mm and $z = 0$ mm).

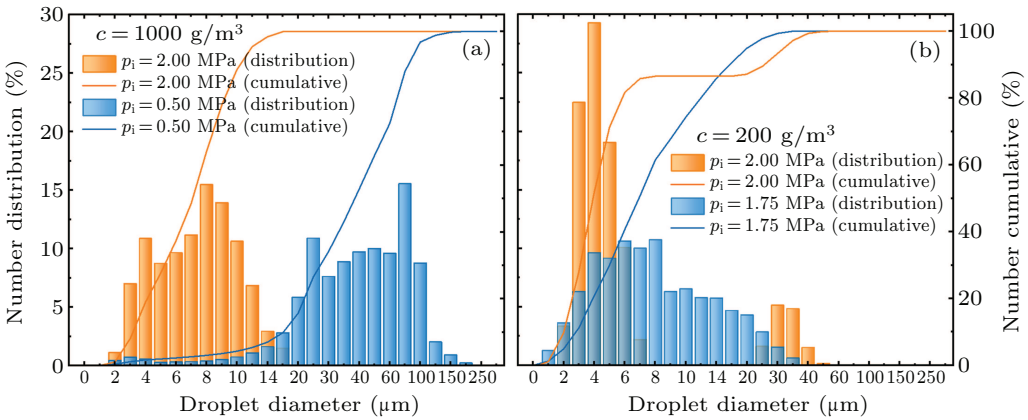


Fig. 7. Comparisons among droplet size distributions and cumulative number percentages of 1-butanol spray for different injection pressures at $c = 1000$ g/m^3 (a) and 200 g/m^3 (b) ($x = 100$ mm and $z = 0$ mm).

The difference in viscosity between butanol and water may be a key factor influencing this phenomenon. The lower viscosity of water enables the aggregation effect in the spray process to be more prominent and to occur easily at smaller mass concentrations. Based on the dimensionless analysis, it is suggested that the high-speed airflow along with high *We* significantly promotes the droplet aggregation of low-viscosity liquids. The effect of fuel viscosity is analyzed and discussed in later sections. The D_{32} of the water spray presents an increasing trend; however, it shows a drop at $p_i = 2.00$ MPa, indicating that the high *We* of the airflow improves the probability of collision between the droplets. However, it is further confirmed that the high *We* also promotes the breakup of droplets. This can also be observed in Fig. 7(b).

3.2. Variations of spray particle size in axial direction

Experiments are conducted to compare the droplet diameters and size distributions of three liquid sprays subjected to different injection pressures at different axial distances. Figure 8 shows comparisons of the particle sizes of the test liquids under different injection pressures at axial locations downstream of the nozzle exit ($x = 50$ mm, 100 mm, and 150 mm). The D_{10} and D_{32} both decrease with injection pressure increasing, and their downward trends gradually decrease. This trend is consistent for all the axial locations considered in this work. The magnitude of the particle size reduction is attributed to the increase of the injection pressure. The comparison of the data with respect to D_{10} shows that the droplet size near the nozzle exit is smaller than the droplet size far from the nozzle exit, and the droplet size increases from $x = 50$ mm to 150 mm. This indicates that the increase in axial distance results in enhanced evaporation of tiny droplets, and hence larger droplet sizes are observed. In addition, the low viscosity of the test fuel facilitates the disaggregation of the fuel droplets, thus making it easier to produce smaller droplets. In this process, the probability of collision between the droplets increases and the small droplets tend to collide and re-agglomerate into larger droplets, which was not observed in the experiments with liquids of higher viscosity, however, which is demonstrated more distinctly by the differences in the droplet size distribution and cumulative number percentage in the axial direction, as shown in Fig. 9. The tendency of the droplet size distribution to move toward larger diameters is the main reason for the increase of the diameter in the axial direction. Comparing with the location near the nozzle exit, the spray away from the nozzle exit not only reduces the small sized droplets, but also increases the number of the larger sized droplets, which responsible for the trend seen in Fig. 8.

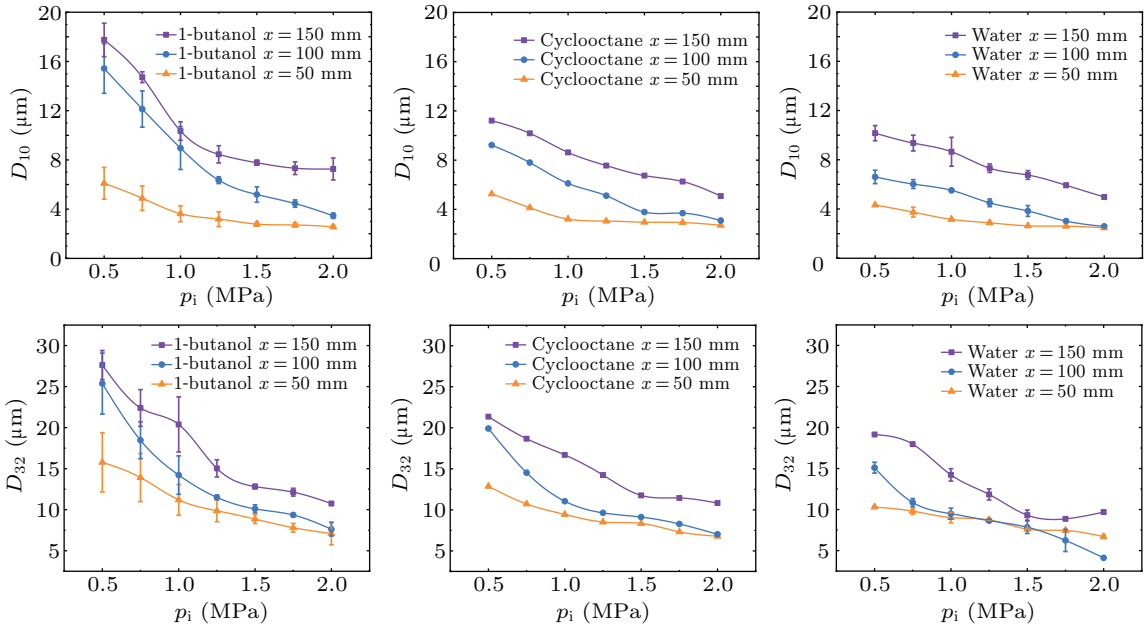


Fig. 8. Comparisons of arithmetic mean droplet diameter (D_{10}, top) and Sauter mean diameter (D_{32}, bottom) of fuel sprays for different values of injection pressure (p_i) at axial locations, $x = 50$ mm, 100 mm, and 150 mm, downstream of the nozzle exit ($c = 1000$ g/m^3; $z = 0$ mm).

At locations close to the nozzle exit ($x = 50$ mm–100 mm), the difference in droplet diameter decreases as the injection pressure increases. The minimum difference is observed at $p_i = 2.00$ MPa. However, it is noteworthy that the difference in droplet size on the spray axis ($x = 100$ mm–150 mm) is different in opposite directions. As the injection pressure increases, the difference augments. The droplet diameter increases along the spray axis due to the aggregation effect. However, the droplet size difference caused by droplet aggregation gradually decreases as the injection pressure increases. It is worth emphasizing that a higher injection pressure promotes breakage of the droplets. This indicates that the increase in injection pressure weakens the effect of small droplet aggregation and promotes droplet fragmentation. In

the "Water $c = 200$ g/m^3" group in Fig. 6(b), the droplet size increases due to droplet aggregation and reaches a peak at $p_i = 1.75$ MPa. The droplet diameter shows a decrease when the injection pressure reaches 2 MPa, when droplet fragmentation dominates. Moreover, the smaller mass concentration also results in a larger airflow driving force per unit mass of fuel, which also has a beneficial effect on droplet fragmentation. Similarly, near the nozzle exit, the higher-velocity airflow breaks the aggregated large droplets into smaller droplets, weakening the effect of aggregation and reducing the difference. However, a significant difference is observed downstream of the nozzle. Figures 9(a) and 9(b) show comparisons of changes of droplet size distribution and cumulative number percentage in the axial direction at low and high injection pressures, respectively. At low injection pressures, the difference in size distribution in the region of $x = 50$ mm–100 mm is evident, indicating a significant aggregation effect. However, a different trend is observed at higher injection pressures. Although D_{10} and D_{32} for $x = 100$ mm are generally higher than those for $x = 50$ mm, the droplet size distribution is more concentrated in the small diameter range. It is observed that the increase in injection pressure inhibits droplet aggregation and promotes breakup. However, the size distribution in the region of $x = 100$ mm–150 mm tends to have a large diameter range, and aggregation occurs again. It is observed that the droplet breakup and aggregation effects coexist and suppress each other in the whole spraying process, which affects the spraying characteristics of the fuel. Except for the water droplets, the curves quantified and compared for D_{32} in Fig. 8 were similar to those for D_{10}. When the injection pressure increases to 1.75 MPa, the droplet particle size decreases near the nozzle exit ($x = 50$ mm–100 mm). Furthermore, the trend is more prominent as the injection pressure increases, owing to the significant contribution of the majority of the small droplets. This indicates that droplet breakup and atomization dominate at this stage. The beneficial effects of the low viscosity of the liquid and high *Ma* airflow on the fuel spray are further demonstrated. However, the droplet diameter at $x = 150$ mm increases slightly, indicating that the droplet fragmentation consumes the airflow driving force, and the aggregation effect continues to dominate as the axial distance increases. At $x = 50$ mm–100 mm, the increase of small droplets further promotes the aggregation of droplets.

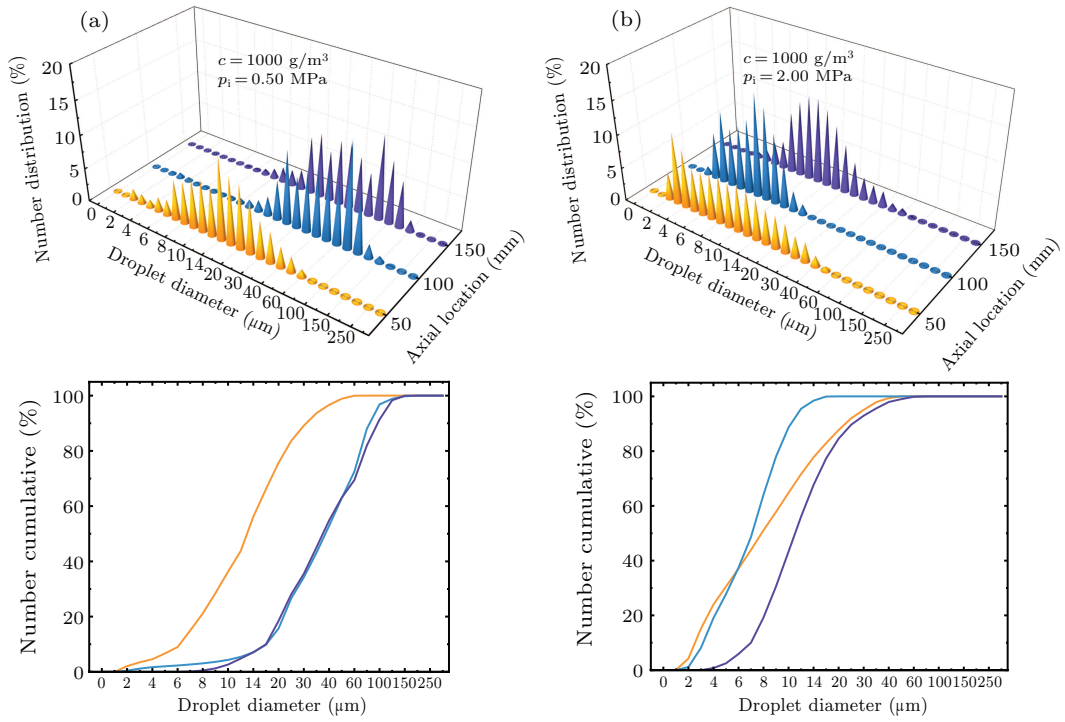


Fig. 9. Comparison of droplet size distribution and cumulative number percentage of 1-butanol spray for different axial locations at $p_i = 0.50$ MPa (a) and 2.00 MPa (b) ($c = 1000$ g/m^3; $z = 0$ mm).

Comparisons of D_{32} between liquids with different viscosities under various injection pressures at axial locations, $x = 50$ mm, 100 mm, and 150 mm, are shown in Fig. 10. The variation in D_{32} is influenced by the viscosity of the test liquid. At lower injection pressures, the experimental results have larger error bars. The main reason is that the low injection pressure produces a lower airflow driving force and a small and uneven force per unit mass of fuel at the moment of airflow driving, so any slight fluctuation in injection pressure will affect the spraying effect. This is also illustrated by the significant effect of lower injection pressure on droplet diameter. As shown in Table 2, the viscosity of the tested liquids is in the order of 1-butanol > cyclooctane > water; therefore, larger droplet sizes are observed in the experiments for the samples

with higher viscosities. The same trend is observed in the axial direction downstream of the nozzle exit. However, the breakup and atomization of droplets and the aggregation effect affecte the variations in the droplet size with increasing axial distance in the whole spray development process. Less viscous fuels produce smaller droplets, which is consistent with the previous analysis. Further analysis demonstrates that the less viscous fuel is more easily broken into small droplets after experiencing the high-speed airflow, and the atomization effect is more evident. In the spraying process, viscosity affects the droplet formation characteristics. In addition, the increase of injection pressure has a more significant effect on the reduction in droplet diameter for high-viscosity liquids.

The effect of droplet aggregation on the fuel spray characteristics is significant, and collision-induced fragmentation and aggregation have a significant effect on the droplet size distribution. The droplet position distribution will have an effect on the subsequent spray combustion, including ignition energy and ignition position. Through the distribution of droplets at different positions, the optimal ignition conditions are set up, and the spray position or ignition state is changed appropriately to achieve the best combustion state and improve the combustion efficiency. The work done in the confined space is enhanced, and the heating effect is obvious. In the open environment, the velocity of the flow field increases, and the thrust force is enhanced. Therefore, the aggregation effect of droplets is an important factor when exploring the spray characteristics and flow field state.

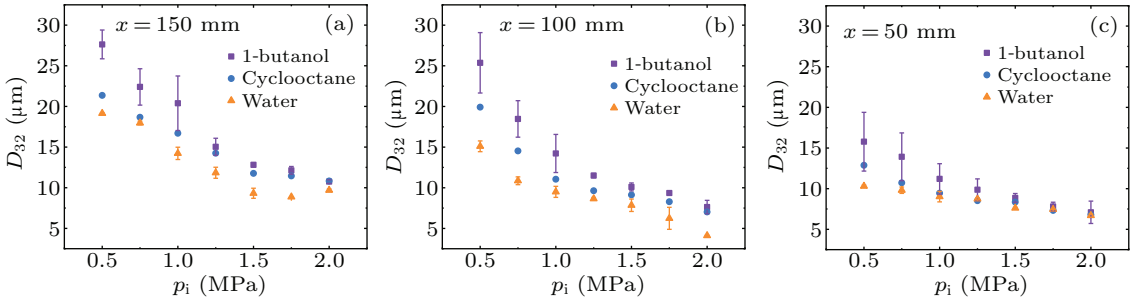


Fig. 10. Effects of viscosity on Sauter mean diameter (D_{32}) for different injection pressures (p_i) at axial locations, $x = 50$ mm (a), 100 mm (b), and 150 mm (c), downstream of nozzle exit ($c = 1000$ g/m^3; $z = 0$ mm).

3.3. Variations of spray particle size in radial direction

Experiments are conducted to compare the droplet diameter and size distribution of three liquid sprays subjected to different injection pressures at different radial distances. Figure 11 shows the comparisons of the particle sizes of the test liquids under various injection pressures at radial locations $z = 0$ mm, 25 mm, and 50 mm for the axial location $x = 100$ mm. The trend of the decreasing of size of the droplet at different radial locations with injection pressure increasing is consistent with that reported in previous study. The D_{10} and D_{32} decrease from the spray axis ($z = 0$ mm) toward the spray boundary, and the decrease is gradually reduced. After the entrainment effect is rapidly enhanced, the cloud diffuses in the radial direction in the spraying process, increasing the number of smaller droplets. Furthermore, owing to the effect of air turbulence and entrainment, the large sized droplets move axially with the airflow, whereas the small droplet population deviates outward. The fuel at the spray boundary is broken into a fewer number of droplets. The density of droplets in the peripheral region is less than that in the axis region, resulting in insignificant droplet aggregation. This results in the droplet size decreasing in the radial direction. The droplet size distribution of 1-butanol in the radial direction at $c = 1000$ g/m^3 and $p_i = 0.5$ MPa is compared as shown in Fig. 12(a). It can be clearly observed that the size distribution of the droplet population at the spray boundary shifts toward a smaller diameter range. The decreasing trends of D_{10} and D_{32} presented in Fig. 11 are mainly due to the increase in the number of smaller droplets. This is also present in other cases.

At $z = 50$ mm, the decrease in the droplet size becomes smaller than that at $z = 0$ mm and 25 mm. The main reason for this phenomenon is that the variation of the spray from the spray axis to the spray boundary is due to radial expansion and the distance from the spray axis, which leads to the decrease of the turbulent intensity of the airflow, and turbulent intensity is an important parameter affecting droplet breakup and atomization. Furthermore, in all the cases investigated, the difference in droplet diameter in the radial direction gradually narrows as the injection pressure increases. This indicates that the injection pressure significantly promotes more intense droplet breakup and atomization near the spray axis compared with that in spray boundary region. It is noteworthy that an increasing trend in the droplet diameter in the radial direction is observed at higher injection pressures. When the injection pressure is high, the droplet diameter near the spray axis is smaller than that at the spray boundary, which is particularly evident in the case of low-viscosity fuels. It is clearly observed in the spray of water droplets in Fig. 11. The stronger droplet fragmentation near the spray axis region increases the outward deflection of smaller droplets and the droplet density at the spray boundary. The larger spray pressure also strengthens the radial turbulence intensity, leading to a significant aggregation

effect. This indicates that the promotion of breakup via the high-*Ma* airflow is significant near the spray axis. To some extent, the trend of droplet reduction in the radial direction can be reversed to achieve good atomization in the axial flow region. This can be more intuitively explained by comparing the changes in the droplet size distribution and cumulative number percentage in the radial direction under low and high injection pressures as shown in Figs. 12(a) and 12(b), respectively. Although the high injection pressure also promotes the size distribution at $z = 50$ mm to shift toward smaller diameters, the effect is subtle. By contrast, the size distribution at $z = 0$ mm exhibits a significant shift. Therefore, the low viscosity of the liquid and high *Ma* airflow have equally beneficial effects in the radial direction.

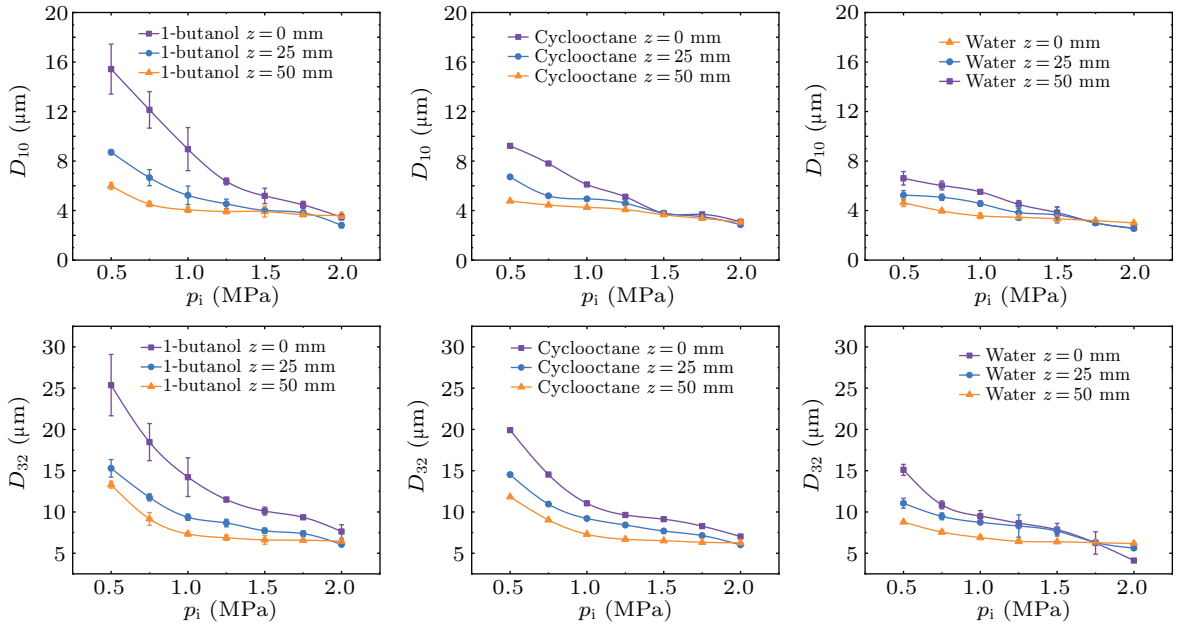


Fig. 11. Comparisons of arithmetic mean droplet diameter (D_{10}, top) and Sauter mean diameter (D_{32}, bottom) of fuel sprays for different injection pressures (p_i) at radial location $z = 0$ mm, 25 mm, and 50 mm for $c = 1000$ g/m^3, $x = 100$ mm.

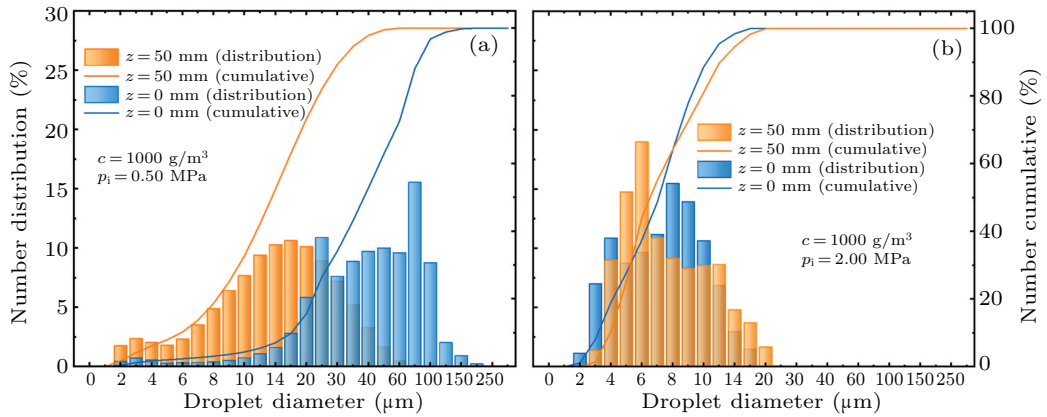


Fig. 12. Comparisons of droplet size distribution and cumulative number percentage of 1-butanol spray for different radial locations at $p_i = 0.50$ MPa (a) and 2.00 MPa (b) for $c = 1000$ g/m^3, $x = 100$ mm.

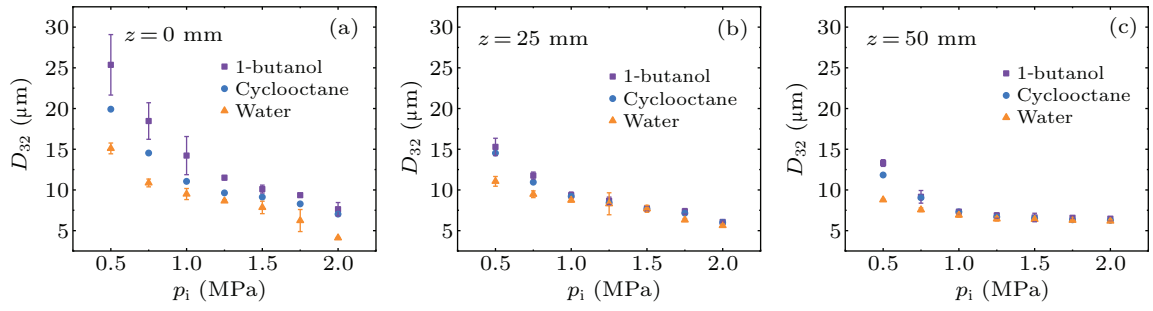


Fig. 13. Effects of viscosity on Sauter mean diameter (D_{32}) for different injection pressures (p_i) at radial locations $z = 0$ mm (a), 25 mm (b), and 50 mm (c) for $c = 1000$ g/m^3, $x = 100$ mm.

Comparison of D_{32} between liquids with different viscosities under different injection pressures at radial locations $z = 0$ mm, 25 mm, and 50 mm is shown in Fig. 13. The droplet diameter variation follows the same trend as the fuel viscosity, with a lower viscosity liquid possessing a better breakup and atomization in the radial position, which is consistent with that observed in the spray axis area. Change in the droplet size during spray development does not change the effect of the intrinsic viscosity of the liquid on the atomization effect. Moreover, the effect of the injection pressure on the difference between the droplet diameters is more evident in the sprays of high-viscosity liquids. As shown in Figs. 10 and 13, low-viscosity fluids appear to change smoothly with injection pressure increasing at an earlier stage compared with the high-viscosity fluids. It can be seen from Fig. 13 that the effect of liquid viscosity on droplet particle size varies at different radial positions. The differences in radial droplet size among different viscosity fuels are mainly in the region close to the spray axis, while the difference at the spray boundary is not significant. Owing to air entrainment, the larger droplet sizes move axially with the air stream, and the increase in spray pressure mainly promotes the breakup of droplets close to the spray axis. This is especially true for the larger viscosity liquids, where the larger density droplet groups move along the axial direction. Meanwhile, smaller droplets shifted toward the spray boundary are affected by the weaker turbulence intensity, and the effect of fuel viscosity on particle size difference is much less. Although the increased injection pressure also enhances the radial driving force, the overall low density and small particle size of droplets at the spray boundary make the particle size difference of different viscosity fuels insignificant.

4. Conclusions

The effects of mass concentration and injection pressure on the spray characteristics of fuels in a 20-L spray chamber are investigated, which are quantified and compared for three different test fuels. To this end, test experiments are conducted at seven injection pressures ($p_i = 0.50$, 0.75, 1.00, 1.25, 1.50, 1.75, and 2.00 MPa) by using high-speed airflow as the driving force. The characteristics of the spray droplets are measured by using Malvern Panalytical Spraytec at three axial locations ($x = 50$, 100, and 150 mm) and three radial locations ($z = 0$, 25, and 50 mm) downstream of the nozzle exit. From the results, the main conclusions are obtained below.

(I) The increase of mass concentration has an inhibitory effect on atomization, and the variation in the particle size with mass concentration can be fitted linearly. Moreover, the mass concentration significantly affects the particle size of the spray droplet at low injection pressures.

(II) The increase of injection pressure enhances *Ma* and driving force of the airflow, which promotes droplet breakup; however, the effect gradually diminishes. Similarly, the injection pressure significantly affects the spraying effect at high mass concentration.

(III) In comparison with the mass concentration, the injection pressure dominates the spraying process and has a greater influence on the spraying effect, reducing the droplet diameter to its limit and weakening the effect of the mass concentration.

(IV) Although the low mass concentration and high injection pressure promote droplet breakup, they also increase the probability of collision between the small droplets and increases the likelihood of the aggregation effect. This effect is more prominent in low-viscosity fuels, which was not previously observed in higher-viscosity liquid sprays.

(V) In the axial direction, the droplets tend to increase owing to the aggregation effect. Moreover, because of the air turbulence and entrainment effect, the large droplets develop in the axial direction, whereas the small droplet population deviates outward. Therefore, the droplet diameter tends to decrease in the radial direction; however, the trend is reversed when the injection pressure increases to a certain level.

(VI) The high-speed airflow significantly promotes the breakup of droplets in the region close to the nozzle exit and spray axis and suppresses the aggregation effect to a certain extent, where the difference in droplet diameter gradually decreases with injection pressure increasing. The effect is minimal at the spray boundary and far from the nozzle outlet.

(VII) Droplet fragmentation and aggregation effects coexist and mutually inhibit in the whole spraying process. Nevertheless, the trend of the viscosity of the fuel on the droplet size does not change. The low-viscosity fuels exhibit better atomization, and smoother changes are observed with injection pressure increasing at an earlier stage compared with the high-viscosity fluids.

Acknowledgement

Project supported by the Young Scientists Fund of National Natural Science Foundation of China (Grant No. 11802136).

References

[1] Kondrasheva N K and Kondrashev D A 2015 *Petroleum Chemistry* **55** 68
[2] Devarajan Y, Beemkumar N, Ganesan S and Arunkumar T 2020 *Fuel* **268** 117254
[3] Feng Z, Zhan C, Tang C, Yang K and Huang Z 2016 *Energy* **112** 549
[4] Shi C, He N, Zhong J, Zhou F, Zhang W, Zhang Y, Yuan S, Shen Y and Wang R 2015 *Automotive Engineering* **37** 1103 (in Chinese)
[5] Souza de Carvalho M J, Seidl P R, Pereira Belchior C R and Sodre J R 2010 *Tribology International* **43** 2298
[6] Wang D, Ye N, Fu Y and Zhang X 2016 *Lubrication Engineering* **41** 132 (in Chinese)
[7] Li X, Li T and Xu M 2019 *Experiments in Fluids* **60** 109
[8] Kang D, Kim D, Kalaskar V, Violi A and Boehman A L 2019 *Fuel* **239** 1388

[9] Wang Z, Alswat M, Yu G, Allehaibi M O and Metghalchi H 2017 *Fuel* **209** 529
[10] Lobo P, Rye L, Williams P I, Christie S, Uryga-Bugajska I, Wilson C W, Hagen D E, Whitefield P D, Blakey S, Coe H, Raper D and Pourkashanian M 2012 *Environmental Science & Technology* **46** 10805
[11] Badami M, Nuccio P, Pastrone D and Signoretto A 2014 *Energy Conversion and Management* **82** 219
[12] Reitz R D and Duraisamy G 2015 *Progress in Energy and Combustion Science* **46** 12
[13] Biswas S, Kakati D, Chakraborti P and Banerjee R 2021 *Fuel* **304** 121346
[14] Zhang J L, Chang J T, Ma J C, Wang Y Y and Bao W 2019 *Aerospace Science and Technology* **84** 686
[15] Zhao J Y, Jin N D, Gao Z K, Du M and Wang Z Y 2014 *Chin. Phys. B* **23** 034702
[16] Breitenbach J, Roisman I V and Tropea C 2018 *Experiments in Fluids* **59** 55
[17] Zhang X W, Jin N D, Gao Z K and Zhai L S 2013 *Chin. Phys. Lett.* **30** 050501
[18] Sivakumar D, Vankeswaram S K, Sakthikumar R and Raghunandan B N 2015 *International Journal of Multiphase Flow* **72** 88
[19] Liu N, Wang Z, Sun M, Wang H and Wang B 2018 *Acta Astronautica* **145** 116
[20] Tratnig A and Brenn G 2010 *International Journal of Multiphase Flow* **36** 349
[21] Park S H, Youn I M, Lim Y and Lee C S 2013 *Fuel Processing Technology* **106** 392
[22] Han D, Wang C H, Duan Y Z, Tian Z S and Huang Z 2014 *Energy* **75** 513
[23] Kim H J, Park S H and Lee C S 2016 *Energy* **107** 572
[24] Fu W, Li F Y, Meng K S, Liu Y J, Shi W D and Lin Q Z 2019 *Energy* **185** 77
[25] Lin K C, Jackson K, Behdadnia R, Jackson T A, Ma F H and Yang V 2010 *J. Propul. Power* **26** 1161
[26] Kannaiyan K and Sadr R 2014 *Energy Conversion and Management* **88** 1060
[27] Kannaiyan K and Sadr R 2021 *Fuel* **294** 120467
[28] Chang F, Luo H, Zhan C, Nishida K and Ogata Y 2021 *Fuel* **299** 120894
[29] Qi W, Zhou Y and Zhang Y 2020 *Experiments in Fluids* **61** 87
[30] Mittal M 2017 *Journal of Loss Prevention in the Process Industries* **46** 200
[31] Wang C, Cao J and Long W 2019 *Applied Thermal Engineering* **159** 113975
[32] Bai J S, Zhang Z J, Li P and Zhong M 2006 *Chin. Phys.* **15** 22
[33] Wang T, Bai J S, Li P and Zhong M 2009 *Chin. Phys. B* **18** 1127
[34] Zhao K, She Y Z, Jiang Y L, Qin J and Zhang Z H 2019 *Acta Phys. Sin.* **68** 244401 (in Chinese)
[35] Wang B, Wang J D, Chen D R, Sun N and Wang T 2017 *Chin. Phys. B* **26** 054701
[36] Yuan S, Ji C, Han H, Sun Y and Mashuga C V 2021 *Process Safety and Environmental Protection* **146** 499
[37] Liu X, Wang Y and Zhang Q 2016 *Fuel* **165** 279
[38] Hu E, Tian H, Zhang X, Li X and Huang Z 2017 *Fuel* **188** 90
[39] Liu X, Zhang Q and Wang Y 2015 *Process Safety and Environmental Protection* **95** 184
[40] Lyu Q, Zang X, Pan X, Ma P, Yu H and Jiang J 2019 *Explosion and Shock Waves* **39** 146 (in Chinese)
[41] Wu F, Yu H, Pan X, Zang X, Hua M, Wang H and Jiang J 2022 *Process Safety and Environmental Protection* **161** 162
[42] Wigley G, Goodwin M, Pitcher G and Blondel D 2004 *Experiments in Fluids* **36** 565
[43] Liu X, Zhang Q and Wang Y 2014 *Industrial & Engineering Chemistry Research* **53** 12856
[44] Sun X, Tang H and Dai J 2007 *Opt. Express* **15** 11507
[45] Ma L and Hanson R K 2005 *Appl. Phys. B* **81** 567
[46] Semião V, Andrade P and Carvalho M D G 1996 *Fuel* **75** 1707
[47] Zhang Q K, Xia J, He Z Y, Wang J P, Liu R, Zheng L, Qian Y, Ju D H and Lu X C 2021 *Energy* **218** 119474